Vol. 84 (1993) *ACTA PHYSICA POLONICA A* No. 1

Proceedings of the VI International School on Magnetism, Białowieża '92

MUON SPIN ROTATION IN HIGH T_c SUPERCONDUCTORS

A. GOLNIK

Institute of Experimental Physics, Warsaw University
Hoża 69, 00-681 Warszawa, Poland

A review of the muon spin rotation studies on high temperature superconductors is presented, with the special emphasis on the investigations of the magnetic ordering and spin–spin correlations in these materials.

PACS numbers: 76.75.+i, 74.72.–h, 74.25.Ha

1. Introduction

The successful application of the muon spectroscopy in the physics of high temperature superconductors, particularly in studies of the penetration depth and magnetic phase diagram, demonstrated the power of the muon spin rotation (μSR) method by investigations of local magnetic fields and weak magnetism.

The review of the μSR studies on high temperature superconductors presented in this paper will be focused on the subject of spin ordering phenomena in these materials. The discussion will be illustrated mainly with the results of μSR experiments done at the Paul Scherrer Institute (PSI) in Villigen, Switzerland, by the group of physicists from the University of Konstanz (Germany) in which the author has taken part.

The review will be preceded by a short description of the μSR method. More details about the method can be found in reviews [1, 2].

2. Muon spin rotation techniques

Muons (μ^+, μ^-), the point-like elementary particles locate in the family of leptons between electrons (e^+, e^-) and taons (τ^+, τ^-). The muon is about 206 times heavier than the electron and almost 9 times lighter than the proton. Therefore, the positive muon is often considered in solids as a light isotope of hydrogen.

The scope of this paper will be restricted to the experiments with positive muons only. In solids the positive muons occupy mainly the interstitial positions, providing information about the internal magnetic field at such sites. The negative muons are rapidly captured into the $1s$ atomic orbital of the host atoms. μ^- on the

1*s* orbital is much closer to the nucleus than 1*s* electrons and therefore interacts much stronger with the nucleus. This interaction reduces the lifetime of μ^- in solids. In addition the asymmetry observed in μ^-SR is small. Therefore, in the μSR studies of magnetism, the negative muons were rarely used. The interest to μ^-SR experiments have increased recently, especially for high T_c superconductors, see e.g. [3]. However, these experiments will not be discussed in this paper.

The muon spectroscopy is based on the two fundamental physical phenomena, both of them being the result of the violation of parity conservation in the weak interactions:

- The muons resulting from the pion decay are 100% spin polarized (in the center of mass system).
- The positron resulting from the muon decay are emitted anisotropically with respect to the muon spin direction.

2.1. Muon implantation

The polarized muon beams are usually produced in the "meson factories" using the proton accelerators (more than 500 MeV). For solid state physicists the main difference between the two types of muon beams, available in practice, is the amount of target material needed for studies.

- The surface muon beams (Arizona beam), where muons result from the decay of pions that come to rest in the production target, supply muons with the momentum of 28.6 MeV/c and kinetic energy of 4.1 MeV. Such muons stop in the matter at the depth about 0.15 g/cm^2, which for the sample density of 5 g/cm^3 corresponds to the depth of 0.3 mm. The stopping depth could be reduced using a degrader in front of the sample, but depth spreadout (due to the range straggling typically 10% of the nominal range) still limits the use of μSR technique to bulk samples. The μSR application for thin films and in surface physics should be possible with the cold muon (thermal muon) beams, which are recently under development.
- The decay channel beams, where the pions decay in flight, provide muons with much higher momentum (105–210 MeV/c), therefore the muon stopping depth is also much higher. Even using the degrader one needs the samples a few millimeters thick. This is due to the range straggling.

Polarized muons implanted into the sample come to rest within the time of about 10^{-11}–10^{-10} s (i.e. faster than the time resolution of μSR detection systems), practically without loosing their polarization.

The muon stopping process in solids (especially in semiconductors) is discussed in more details in the review article of Patterson [4]. Here we state only the main points of this discussion concerning the influence of radiation damages (created during implantation) on the implanted muon.

Typical muon fluxes are of the order of 10^8 incoming muons per cm^2 per one experiment (1 h). The accumulated-defect concentration by 20 h experiment would be of the order of 5×10^{11} cm^{-3}. At a typical muon diffusion rate the muon

would need several hundreds of μs to find a defect. This time is much longer than the muon lifetime. Both the analytical calculations of Brice [5] and the numerical simulations done by Patterson [4] indicate that the distance between the muon stopping site and the last displaced atom is of the order of 10 μm. So the interaction of the muon with the radiation damage created by itself is very improbable.

2.2 Muon decay

The mean lifetime of the muon is 2.1971 μs. μ^+ decays by the weak interaction into a positron, an electron-neutrino and a muon-antineutrino:

$$\mu^+ \rightarrow e^+ + \nu_e + \underline{\nu}_\mu. \tag{1}$$

The only particle from the μ^+ decay, that is observed in the μSR experiment, is positron. Since the μ^+ decay is a three-body decay, the resulting positron can have energy from 0 to the maximal energy of 52.3 keV. The probability of the positron emission in the given direction depends on its energy and the angle Θ between this direction and the spin of muon at the time of decay. After integrating over the whole possible positron energies, one obtains this probability in the following form:

$$\mathrm{d}W = \{(1/\tau_\mu)[1 + (1/3)\cos\Theta]/2\}\mathrm{d}\cos\Theta. \tag{2}$$

The 1/3 average anisotropy of the muon decay in this formula is the factor, which enables the detection of muon spin direction in all the μSR experiments.

2.3. Spin precession and depolarization function

The muon placed in a steady magnetic field with the spin not parallel to the field direction exhibits the spin precession. The Larmor frequency is given by the muon gyromagnetic ratio

$$\gamma_\mu/2\pi = 135.534 \text{ MIIz/T}. \tag{3}$$

This value should be compared with that resulting from the Bohr magneton $\mu_B/h \approx 14$ GHz/T and nuclear magneton $\mu_N/h \approx 7.6$ MIIz/T.

The magnetic field acting on the muon can be of a different origin:

- external,
- demagnetization (macroscopic fields proportional to magnetic susceptibility of the solid depending on the sample shape and its orientation versus magnetic field),
- nuclear dipolar (superposition of local dipolar fields from the spins of nuclei),
- electron dipolar (superposition of local dipolar fields from the spins of localized electrons),
- hyperfine (contact term of dipolar interaction with the electron spin density at the muon site, resulting in Knight shift in metals or supertransferred field in insulators).

During the muon lifetime the muon spin polarization not only precesses in the magnetic field but is also lost in the depolarization process. Like in the magnetic resonance experiments, where the transverse and longitudinal relaxation are different, in μSR the transverse and longitudinal depolarization should be considered separately. Since in μSR the depolarizations are not necessarily exponential, they are usually described by the depolarization functions $G_x(t)$ and $G_z(t)$, respectively.

2.4. Time differential spectroscopy

In this conventional (but still most often used) μSR technique, the amount of positrons emitted in a given direction is measured as a function of the time between the muon implantation and the emission of positron.

Usually the incoming muon passes a very thin scintillation counter (M-counter). The impulse from this counter starts the electronic clock. The clock is stopped by the impulse from one of the positron counters placed at the certain angle with respect to the initial polarization of the muon beam. The events are histogrammed as a function of clock time for each counter. This method is suitable for dc muon beams, but involves the requirement that *only one muon can be present at the same time in the sample* (otherwise the event have to be ignored). This condition demands the use of on-line, veto electronic system and reduces the count accumulation rates.

On the pulsed muon beams the method could be modified by starting the clock with the pulse coming from the accelerator and using multiple stops. But then, the time resolution is reduced by the time-width of incoming muon burst.

For each positron counter, the following expression gives the number of events as a function of time between the incoming muon pulse and the registration of a decay positron:

$$N(t) = N_0 \exp(-t/\tau_\mu)[1 + A(t)] + B, \tag{4}$$

where N_0 and B are normalization and background constants. The background results from the events where the start-stop signals were not correlated (e.g., positrons from the muon stopped somewhere outside the sample). $A(t)$ is the asymmetry function, which contains the information about precession and depolarization. It depends also on experiment geometry and effective asymmetry A.

Since N_0 and B do not contain physical information about studied material, usually only the asymmetry part of the μSR spectrum, (i.e. $A(t)$), is plotted on the figures.

2.5. Transverse field μSR

This geometry is particularly suitable for the studies of the field distribution in solids in response to the externally applied fields. Additionally the experiments in this geometry can provide the information about dynamical processes, like muon diffusion or spin fluctuations.

The initial polarization of the muon beam should be perpendicular to the direction of the external magnetic field, therefore the muon spin will precess in the plane perpendicular to the field direction (Fig. 1).

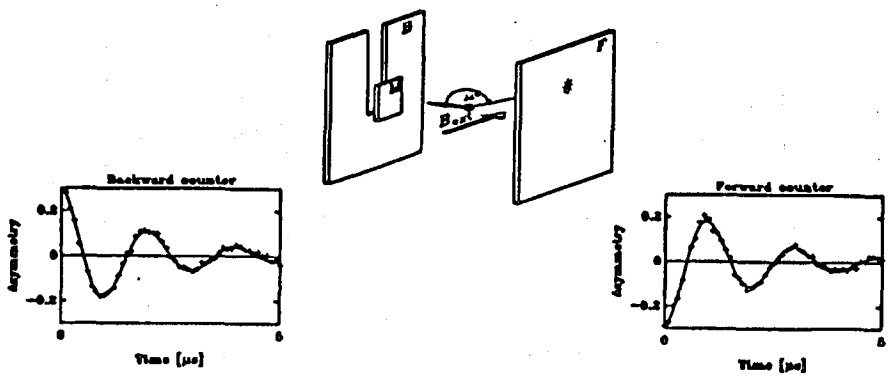

Fig. 1. Schematic representation of the transverse field μSR configuration and sample μSR spectra in the forward and backward counters.

The asymmetry part of the μSR spectrum will then contain the precession signal

$$A(t) = AG_x(t)\cos(\omega t + \phi), \tag{5}$$

where A is the effective asymmetry factor. It includes the corrections to the muon decay asymmetry (1/3) due to energy dependence of counter efficiency and incomplete beam polarization. $G_x(t)$ is the transverse depolarization function, containing the physically interesting information about field distribution and dynamic processes. ω is given by the muon precession frequency in the internal magnetic field (see Eq. (3)). ϕ is the phase, which depends on the initial angle between the muon spin and the direction towards a positron counter.

In the static case the magnetic field at the muon stopping site does not change within the muon lifetime. Then, the transverse relaxation function is given by the distribution of the magnetic fields at muon stopping sites. If this field distribution has a Gaussian shape with the width ΔB, then G_x has the form

$$G_x(t) = \exp[(1/2)\sigma^2 t^2], \tag{6}$$

where $\sigma = \gamma_\mu \Delta B$ ($\gamma_\mu = 851.6\ \mu s^{-1}/T$).

In the dynamic case, when the local fields at the muon site fluctuate or the muon diffuses through the solid, the depolarization is weakened in the effect analogous to "motional narrowing" observed in NMR and EPR. For the Gaussian field distribution the G_x function can be then well approximated [6] in the form

$$G_x(t) = \exp\{-\sigma^2\tau^2[\exp(-t/\tau) - 1 + t/\tau]\}, \tag{7}$$

where τ is the characteristic time of dynamic process (diffusion, fluctuation).

The example of the Gaussian depolarization function and its "motional narrowing" is shown in Fig. 2.

The fast fluctuation limit ($\sigma\tau \ll 1$) of the above depolarization function is exponential

$$G_x(t) = \exp(-\lambda t), \tag{8}$$

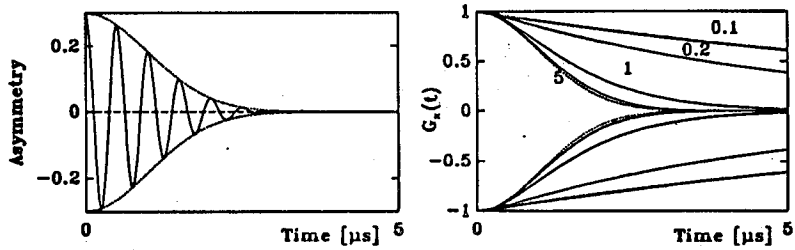

Fig. 2. The muon asymmetry $A(t)$ for the static case ($\nu = 2$ MHz and $\sigma = 1\ \mu s^{-1}$ ($B \approx 15$ mT and $\Delta B = 1.2$ mT) (left) and the envelope function $G_x(t)$ in case of "motional narrowing" (right) (for $\tau = 5,\ 1,\ 0.2,\ 0.1\ \mu s$, respectively).

where

$$\lambda = \sigma^2 \tau. \tag{9}$$

In the cases when the field distribution has a more complicated shape (e.g., the case of vortex state of superconductors), this distribution should be derived from the real part of the Fourier transform of the asymmetry spectrum [7, 8].

2.6. Zero (and longitudinal) field μSR

In that case muons feel only internal fields. Except of the case of monodomain ferromagnetic monocrystals, where the situation is analogous to the transverse field configuration, the internal fields have usually random directions.

For the arbitrary direction of internal field, we have the following situation:

- The precession frequency depends only on the magnitude of resulting field.
- The amplitude of a precession cone depends on an angle between the initial muon spin direction and the magnetic field. When they are parallel or antiparallel (longitudinal configuration) no precession occurs.
- The amplitude of the precession signal recorded by a positron counter depends on the angle between the field (precession) direction and the vector pointing from the muon site towards the detector.

The signal recorded by a positron counter results from an average over all possible fields at the muon stopping sites. Both the precessing (transverse) and non-precessing (longitudinal) parts of a signal have their maximum for counters placed parallel and antiparallel to the initial muon spin polarization. The counters placed at another angles would not record oscillations of another phase, but only of reduced amplitude. (The rotations of opposite sense subtract.)

Therefore for zero field μSR, as well as for longitudinal field μSR there are usually only two positron counters (forward and backward as shown in Fig. 3). The number of counts for this counters is expressed as follows:

$$N^{\pm}(t) = N_0 \exp(-t/\tau_\mu)[1 \pm A G_z(t)] + B, \tag{10}$$

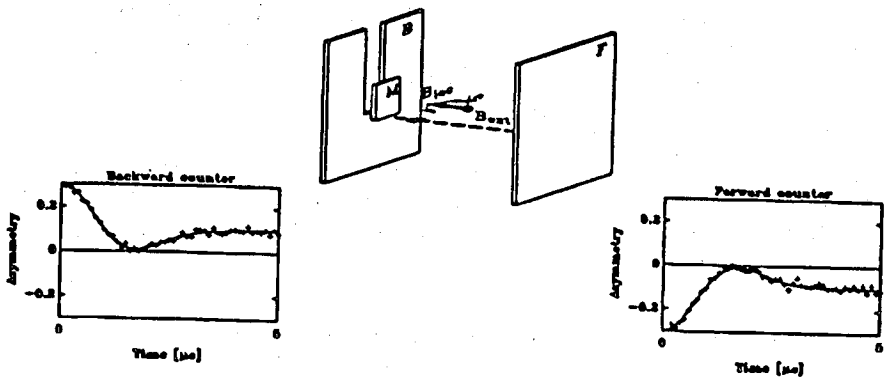

Fig. 3. Schematic representation of a longitudinal μSR geometry (for zero and longitudinal field experiments, $B_{\rm loc}$ and $B_{\rm ext}$, respectively).

where + and − are related to the backward and forward counters, respectively.

By the random distribution of the local field directions, the averaging procedure gives 1/3 of non-precessing (longitudinal) component and 2/3 of a precessing (transverse) component. This is easy to imagine considering the symmetry arguments.

The internal magnetic fields at each muon stopping point result from the summation of individual components (dipolar fields, quadrupolar fields etc.). The non-zero average of such summation points out to the presence of some spontaneous *magnetic order*. It is not necessary that the order would be static. Since the muon is a local probe and its lifetime time is short, the muon would sense also the short distance magnetic order or even only the magnetic correlations, if their characteristic lifetime (fluctuation) is sufficiently long comparing with the muon lifetime.

In case of antiferromagnetic ordering the field at the muon site is non-zero, only if the site is nonsymmetric. So however, the observation of a μSR precession at zero external field implies the presence of some kind of magnetic order, the opposite is not true. If no precession is found, this does not exclude antiferromagnetism.

For magnetically ordered systems the muon stopping sites are often magnetically inequivalent. So more precession frequencies ω_i are expected in the μSR signal, with the amplitudes A_i reflecting the ratio of the site occupancies. For polycrystalline samples, when the directions of internal spontaneous magnetic field are randomly oriented, the muon asymmetry signal is expected in the form

$$A(t) = \sum A_i G_{zi}(t)[1/3 + (2/3)\cos(\omega_i t)]. \tag{11}$$

The 1/3 (longitudinal) constant part of the asymmetry is often omitted in the plots of zero field (ZF) μSR spectra.

If no magnetic order is present in the sample, the vector average of the local fields should be zero. The zero field μSR experiment is however sensitive to the *magnitude* of the field, which does not average to zero. Therefore usually in such cases the 2/3 (transverse) part of the zero field μSR depolarization function G_z

has the form of an overdamped oscillation. The typical example of such a function (for the case of the Gaussian distribution of internal fields, centered at zero) is the Kubo–Toyabe function, originally introduced for NMR in zero magnetic field [9]

$$G_z(t) = 1/3 + (2/3)(1 - \sigma^2 t^2)\exp[(-1/2)\sigma^2 t^2]. \tag{12}$$

The dynamic effects like muon diffusion or spin fluctuations lead again to the "motional narrowing". This effect is schematically depicted in Fig. 4. In the fast diffusion (fluctuation) limit the depolarization function becomes again exponential.

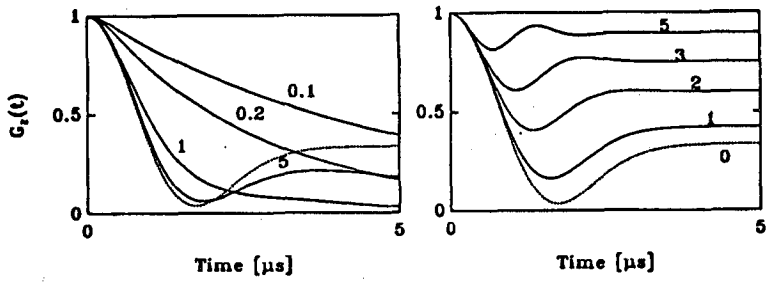

Fig. 4. The Kubo–Toyabe function ($\sigma = 1\ \mu s^{-1}$, $\Delta B = 0.85$ mT) (dashed lines) and the effects of "motional narrowing" (left) $\tau = 5$, 1, 0.2, 0.1 μs and longitudinal field (right) 0, 1, 2, 3 and 5 mT.

The independent method often used to distinguish, whether the internal fields are static or dynamic, is given by the longitudinal field-"decoupling" experiments. The effect of longitudinal field on the Kubo-Toyabe depolarization is illustrated in Fig. 4. When the external field becomes comparable and greater than the amplitude of internal fields, the variation of 2/3 component of Eq. (12) would be damped. The similar decoupling effect would occur in dynamic ("fluctuation narrowing") case for much higher fields comparable with fluctuating internal fields.

2.7. Integral techniques

Among the integral μSR techniques like stroboscopic μSR and magnetic resonance, the one of increasing importance is the avoided-level-crossing technique (or muon level crossing resonance, μLCR) proposed for μSR by Abragam [10] and demonstrated the first time by Kreitzman et al. [11].

In the longitudinal field configuration the initial spin state of muon is already the eigenstate. The energy splitting of the two muon spin eigenstates is given by the field strength. When the energy splitting of the muon spin states becomes equal to the splitting of the energy levels of another system (usually the neighboring nuclei), the weak coupling between these two systems mixes their quantum states. These changes the transition probability between muon levels (longitudinal relaxation) and introduces corrections to the energy of the levels that avoid their crossing (the phenomenon of level repulsion). Such phenomenon could be recorded

as the characteristic resonance feature on the magnetic field dependence of the time-integrated muon asymmetry.

More detailed description of the method can be find e.g., in the article of Kreitzman [12].

2.8. Muon site and chemistry of muon binding

The complete analysis of a μSR experiment should include also the problem of muon localization, what involves the questions of:

- spatial position of muon in crystal lattice,
- the charge state of muonic center (electronic configuration, muon binding),
- influence of the muon on the surrounding lattice,
- possibility of muon motion between equivalent sites (diffusion).

The direct method for muon site determination is given by the channeling experiments (called also the muon-decay-blocking experiments) [13]. Since this method requires the use of large, good quality single crystals, the other indirect methods are much more often used. More recently the avoided-level-crossing technique becomes wider used for the study of the environment of the stopped muon.

At the last stage of muon stopping process a large amount of electrons or holes would be available in the vicinity. Therefore the positive muon can easily capture an electron forming a neutrally charged bound state analogous to the atom of hydrogen. Such a bound state is called *muonium* (Mu) or the *paramagnetic* state of muon, since its behavior in the magnetic field is dominated by the spin of electron ($\mu_B/h \approx 14$ GHz/T). The hyperfine (contact) interaction between the electron and the muon spin is of Heisenberg form, with the "exchange" constant being equal to 4.46330288 GHz for the muonium in vacuum.

The therm "*diamagnetic state of the muon*" is then reserved for any center where the observed muon spin precession occurs, with the frequency given by the muon gyromagnetic ratio ($\gamma_\mu/2\pi \approx 135$ MHz/T). Such centers are usually assigned to the positive charge state of single μ^+.

Since the muon in solid could be considered as light isotope of proton, the problem of the muon bonding is analogous to the problem of hydrogen in solids. However, some differences between those two species in solids could result from the fact that sometimes the muon may not reach his final position within his lifetime, whereas the diffused hydrogen is usually found in its most stable site.

There are some hints what muon states should be expected in different materials:

— In metals muons have been found to stop at the interstitial sites in the μ^+ charge state (i.e. do not form the bound state with a single electron). The contact interaction of the muon with the conduction electrons manifests as a Knight shift of a μ^+ precession frequency. The distortion of the surrounding lattice induced by the positive muon leads to the formation of the small polaron state, which often results in the self-trapping of the muon.

— Generally three muon centers have been found in semiconductors, one diamagnetic called μ^+ and two paramagnetic called normal and anomalous muonium (Mu and Mu*). The fractions of the muons found in each of these centers depend on the material itself, its doping (position of Fermi level) and temperature. The detailed discussion of the muonium states in semiconductors and more references may be found in Chap. 4 of the review of Cox [2], in the review article of Patterson [4] and in shorter but more recent articles [14, 15].

— In magnetic oxides the muon bounds to the oxygen atom (see the review [16]) and below 150 K remain localized at about 1 Å from it. Since this case is relevant for high temperature superconductors, it will be discussed in more details.

The muon binding to the oxygen is observed experimentally as an additional hyperfine field. This contact field is transfered by the oxygen p-orbitals polarized by d-electrons of magnetic ions. Such d–p–μ^+ interaction by analogy with the well-known d–p–d superexchange is often called supertransferred. This supertransferred field is usually expressed in the form [16]

$$B_{\mathrm{hf}} = C[(A_\sigma^2 - A_\pi^2)\cos^2\theta_i + A_\pi^2], \tag{13}$$

where A_σ and A_π are the spin polarization magnitudes of the oxygen orbitals p_z and p_x with σ and π symmetry, respectively; θ_i is the angle between the i-th metal ion-oxygen direction and the μ^+-oxygen direction; C is a proportionality constant.

On a search of the muon stopping site, in the case when the spin structure of magnetic materials is known, the calculations of dipolar and supertransferred component of internal magnetic field are performed for different possible muon sites. Such trials are often connected with calculation of potential surface for different positions of μ^+ in the studied material.

3. μSR studies of superconducting properties

The μSR experiments, that studied the *superconductivity* in high T_c superconductors (HTSC), will be only shortly mentioned here. More details can be found in the articles reviewing such studies (see e.g. [17] or earlier reviews based on the results of the TRIUMF group [18]).

The transverse field μSR experiments are very well suited to study the vortex phase of superconductors, since μSR is volume sensitive. The obtained information on the distribution of internal magnetic fields inside superconducting sample could be used e.g., to determine the London penetration depth λ_L.

In the early experiments the mean value of the penetration depth λ_L in ceramic samples was determined from the fit of the Gaussian depolarization function to the measured μSR spectrum. λ_L obtained in this way can be used to determine the superconducting-carrier-concentration n_s. In such a kind of experiments Uemura and co-workers have claimed to find the correlation between T_c and n_s [19].

The more elaborated works interpret the details of the field distribution found in μSR experiments considering the fact that λ_L in HTSC materials is strongly anisotropic. This kind of experiments could be used also to study the

effects of irreversibility (field cooling vs. zero field cooling), flux trapping, and the flux creep.

4. Magnetism of Cu spins

Magnetism seems to play an important role in the HTSC materials. For all classes of these materials the "parent" antiferromagnetic compounds were found (La_2CuO_4 — for the "214" group, [Re]$Ba_2Cu_3O_6$ — for "123" group, yttrium substituted compounds — for Bi and Tl-based HTSC).

The transition from the "parent" insulating and antiferromagnetic phase to the superconducting, metallic state is controlled by the changes of the charge carrier concentration. This concentration could be continuously varied by changing the stoichiometry of the material (oxygen content for "123" compounds and La_2CuO_{4-y} or dopant concentration for other groups).

Both, the charge carriers responsible for superconductivity and the spins of the $3d^9$ shell of Cu^{2+} ions are spatially localized on CuO_2 planes. Such two-dimensional planes are characteristic for the crystal structure of all HTSC materials. Many theoretical models were proposed, which tried to explain the high T_c superconductivity by the pairing mechanism of magnetic origin. In one of such works, Aharony et al. [20] argued that the interactions between charge-carriers and Cu spins should lead to the frustration in the spin system and formation of a spin-glass phase. Therefore in searching for a mechanism of high temperature superconductivity, it seems important to analyze experimentally the magnetic aspects of such phase diagrams.

4.1. "214"

For $La_{2-x}Ba_xCuO_4$ and $La_{2-x}Sr_xCuO_4$ called often "214" compounds, the "parent" magnetic compound is La_2CuO_4. The antiferromagnetism was detected there in the studies of susceptibility [21], neutron scattering [22–24] and μSR [25, 26]. In μSR studies the magnetic ordering was seen as spontaneous oscillations in zero-field experiments. An example of such spectrum is shown in Fig. 5.

The temperature dependence of the μSR frequency provides information about the local fields, so about the magnetic sublattice magnetization. The T = 0 limit of the μSR frequency for La_2CuO_4 was determined for 5.7 MHz, what corresponds to the internal field at the μ^+ site of 42 mT. For the sample prepared in the standard way T_N was about 250 K (compare Fig. 6).

T_N depends strongly on the exact *oxygen stoichiometry* of $La_2CuO_{4+\delta}$. In the original paper of Johnston et al. [21] the maximum of the Néel temperature versus δ was assigned to $\delta = -0.03$, i.e. for $La_2CuO_{3.97}$. The authors claimed that T_N decreases with increasing oxygen content. Such scaling was followed in the μSR works of Uemura et al. [25, 27]. The work of Budnick at al. [28] (where the "oxygen treated" sample had T_N = 300 K, i.e. higher than the standard sample) strongly suggests the other scaling of T_N versus δ. As proposed in [29] the maximum of T_N should be assigned to $\delta = 0$.

The further studies of μSR in $La_{2-x}CuO_{4+\delta}$ could be found in [30, 31]. In [30]

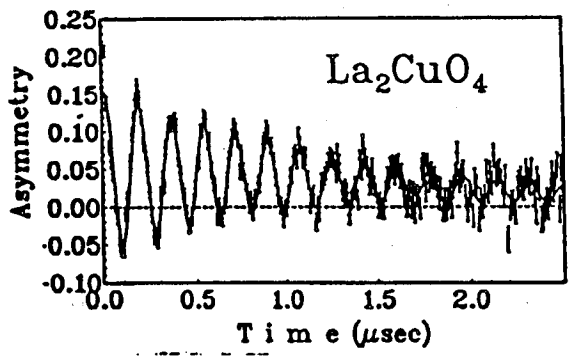

Fig. 5. μSR spectrum of La_2CuO_4 at 11 K [26].

and [32] the temperature dependence of μSR frequency (sublattice magnetization) was analyzed theoretically in terms of anisotropic magnetism of La_2CuO_4.

The most often used method to change the carrier concentration in La_2CuO_4 is however its doping with strontium.

$La_{2-x}Sr_xCuO_4$ is *insulating* for $0 < x < 0.06$. For such materials the magnetism was found in the series of zero field μSR experiments [28, 33, 34]. The example of temperature dependence of μSR frequencies in these materials is shown in Fig. 6.

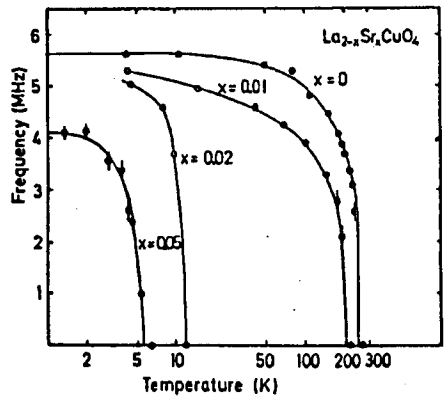

Fig. 6. Temperature dependence of μSR frequencies observed in $La_{2-x}Sr_xCuO_4$. Lines are guides for eye [28].

As could be seen the Sr-doping reduces the Néel temperature of La_2CuO_4. In the range $x \leq 0.01$ this reduction is moderate. Between $x = 0.01$ and $x = 0.02$ a dramatic decrease in transition temperature over more than one order of magnitude is observed. In the range $0.02 < x < 0.05$ the temperature, below which the spontaneous μSR oscillations is observed, changes again moderately.

In contrast to such dramatic changes of the transition temperature, the μSR frequency in the limit of $T = 0$ has changed only from 5.6 MHz for $x = 0$ to 4.1 MHz for $x = 0.05$. Such minor changes of the local magnetic field at the muon site strongly suggest that the whole effect is mainly caused by the changes in the magnetic interactions between Cu spins rather than by the changes of the magnetic moment of the spin itself [28]. The μSR experiment cannot distinguish between long-range ordering and freezing of short-range correlations. The second process may indeed be important for Sr-concentrations with $x \geq 0.02$, therefore the dramatic change of ordering temperature between $x = 0.01$ and 0.02 might correspond to the cross-over from the long-range to short-range type of antiferromagnetic order.

In the theoretical works of Aharony et al. [20] (local approach, similar to those of magnetic polaron) and Schrieffer et al. [35] (spin bag model), it was suggested that the addition of holes to La_2CuO_4 introduces a local ferromagnetic exchange coupling between Cu spins. The resulting frustrations destroy the 3D Néel state characterizing pure La_2CuO_4, and should generate the new 3D spin-glass phase in the range of x between 0.02 and 0.05.

The spontaneous μSR oscillations observed are not typical for the spin-glass phase. However, the experimentally observed fact that the depolarization rate of μSR low temperature oscillations increases with Sr doping, is consistent with the hypothesis of the appearance of ferromagnetic frustrations. The ferromagnetic fluctuations on the antiferromagnetic background, caused by mobile charge carriers, result in inhomogeneous field distribution, which shows up as depolarization of μSR oscillations.

Harshman et al. [33] extended their μSR studies of $La_{2-x}Sr_xCuO_4$ onto longitudinal-field decoupling experiments. Especially, for $x = 0.05$ and temperature just above ordering temperature they found that the μSR signal "is a sum of two components: one (derived from magnetic fluctuations) freezes and yields muon-spin precession at low temperatures, and another (due to a set of apparently stronger moments) that do not yield a precession signal". The first component could be decoupled at the longitudinal field of about 40 mT. The second one could not be completely decoupled even at the fields of 160 mT. The amplitudes of these components were very similar. The observation of two components was attributed to the two different muon stopping sites.

$La_{2-x}Sr_xCuO_4$ becomes *superconducting* for $x > 0.06$. Near the metal–insulator transition some kind of magnetic order was still present. The natural question arises, whether the magnetic moments on Cu ions are still present in the superconducting phase. This question becomes important for the models that derive the mechanism of high T_c superconductivity from magnetic interactions [20], [35].

The first hints of the existence of magnetic correlations in superconducting $La_{1.85}Sr_{0.15}CuO_4$ came from the low-temperature specific heat studies [36]. Later μSR studies of $La_{2-x}Sr_xCuO_4$ with $x > 0.06$ [37–39] confirmed this hypothesis.

Kitazawa and co-workers [37] studied two single crystals with $x = 0.04$ and 0.08. They observed that with decreasing temperature the ZF-μSR spectra changed their character from the Kubo-Toyabe like to the Lorentzian one. The initial asymmetry of the μSR spectra decreased rapidly to about 1/3 of its high

temperature (paramagnetic) value. The authors interpreted the observed ordering as a spin-glass like transition, which for $x = 0.08$ coexists with superconductivity.

Weidinger et al. [38] studied single phase polycrystalline pellets. For the sample with $x = 0.07$ and temperatures $T \leq 1.2$ K μSR oscillation were observed, with finite frequency of $\nu = 1.5$ MIlz and strong Gaussian damping (Fig. 7). As temperature was raised, the shape of a signal changed and the exponentially decaying function became more appropriate. The depolarization rate λ decreased rapidly with increasing temperature and at 4.2 K the spectrum was already dominated by the Kubo–Toyabe decay (caused by the nuclear moments of Cu atoms). For the samples with $x = 0.10$ and 0.15 the signal was exponentially damped even at the lowest temperature of 35 mK and disappeared at about 3.5 K and 2 K, respectively.

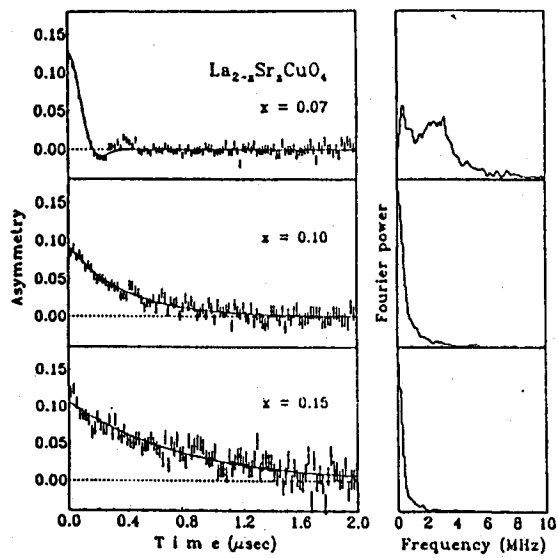

Fig. 7. μSR spectra and their Fourier transforms for $La_{1.93}Sr_{0.07}CuO_4$ at different temperatures [38].

The only way to explain the observation of a strongly damped μSR signal at low temperatures was the conclusion that some magnetic moments of electronic origin are present in superconducting samples and freeze at low temperatures (due to some kind of magnetic correlations), therefore become visible by the μSR method. At higher temperatures the electronic spins fluctuate too fast and the muon spin follows the Kubo–Toyabe relaxation caused by nuclear moments.

Figure 8 shows the phase diagram of $La_{2-x}Sr_xCuO_4$ obtained assuming that the freezing of magnetic correlations observed in superconducting material could be interpreted as a phase transition. The upper part of this diagram shows the ordering temperatures: magnetic (dashed line) and superconducting T_c (solid line). The lower part of Fig. 8 shows the magnitude of the internal magnetic field (in the

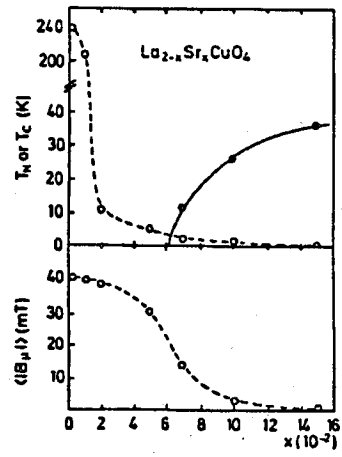

Fig. 8. Phase diagram of $La_{2-x}Sr_xCuO_4$ concerning the magnetic and superconducting properties as a function of the Sr concentration x. Upper part, the magnetic ordering temperature T_N and the superconducting transition temperature T_c. Lower part, the average magnitude of the internal magnetic field at the muon site at 35 mK [38].

low temperature limit). This magnitude for the samples with x between 0 and 0.07 was determined from the frequency of oscillating signal. For the samples with $x = 0.1$ and 0.15, where the signals were exponentially damped, the low temperature limit of depolarization parameter λ was used as an estimate of the width of internal field distribution.

For the $La_{2-x}Sr_xCuO_4$ samples with $x = 0.15$ and the highest T_c (38 K and almost 100% of the Meissner fraction) the signal was of the pure Kubo–Toyabe shape down to 35 mK [40, 41]. This behavior is consistent with the observation that with increasing concentration of mobile holes and increasing T_c the amplitude of magnetic correlations decreases. Therefore for the sample with maximum T_c the damped signal of electronic origin is not observed, either because of the fluctuations are still too fast or because the amplitude of magnetic moments is strongly reduced.

The phase diagram of $La_{2-x}Ba_xCuO_4$ is very similar to those for $La_{2-x}Sr_xCuO_4$. However at $x = 0.13$ $La_{2-x}Ba_xCuO_4$ undergoes the crystallographic phase transition, which suppresses superconductivity. At this concentrations the antiferromagnetic ordering was found in the μSR experiments [42] at temperatures about two times lower than the crystallographic transition from the low-temperature-orthorhombic to low-temperature-tetragonal phase.

4.2. "123"

Although [Re]$Ba_2Cu_3O_7$ compounds (called in jargon the "123" materials) show superconductivity with $T_c \approx 90$ K for most of the rare-earth [Re] substitutions (except for Pr, Ce, Tb and Pm), $YBa_2Cu_3O_{6+x}$ remains the most popular among them. The materials with non-zero spin on Re ion were used rather in the

cases when the magnetic order of the Re spins (or its influence on Cu magnetism) were of interest. These cases will be referred separately in Sec. 6.

The presence of magnetic phase in the Y–Ba–Cu–O system was detected in μSR experiments by Nishida et al. [43, 44] much earlier than the presence of long-range antiferromagnetic order in $YBa_2Cu_3O_6$ was confirmed in neutron scattering experiments [45].

Nishida et al. studied different $YBa_2Cu_3O_{6+x}$ samples prepared by quenching method. For the insulating samples with tetragonal structure ($0.2 < x < 0.38$) they found clear spontaneous μSR oscillations (in a zero-field experiment) with the frequency of about 4 MHz. The Néel temperature (although not sharply pronounced due to the inhomogeneity of the samples) changed drastically from 240 K for $x \approx 0.2$ to 13 K for $x \approx 0.38$. For the orthorhombic sample with $T_c = 60$ K and $x \approx 0.4$ the first evidence for coexistence of superconductivity and spin-glass magnetic state in $YBa_2Cu_3O_{6+x}$ was found.

These studies were extended by Brewer et al. using the method of "weak transverse field μSR" [46]. The magnetic order was there detected by application of a small transverse magnetic field (smaller than the spontaneous local field at the site of muon). The amplitude of the precession signal at the frequency corresponding to the external field is a quantitative measure of the volume fraction magnetically ordered material. The authors used two sets of samples "quenched" and "slow-annealed". The Néel temperature was between 350 and 450 K for $x = 0$ and decreased rapidly around $x \approx 0.3$ for "slow-annealed" and around $x \approx 0.4$ for "quenched" samples. The "slow-annealed" samples with $x = 0.384$ and $x = 0.400$ exhibited coexistence of superconductivity (with $T_c = 25$ K and $T_c = 33$ K) and magnetic order at 10 and 5 K, respectively.

The further studies taken to determine more precisely the phase-diagram [47] and to answer the "coexistence" problem [41, 48] were done using the samples obtained by the "slow-annealing" method, since they were believed to be more homogeneous. However, it is now known (see e.g. [49]) that the oxygen in $YBa_2Cu_3O_{6+x}$ has a tendency to form some kind of superstructure, in the case when its diffusion is allowed in the "slow-annealing" process. (The ordering of oxygen vacancies in "chains" of $YBa_2Cu_3O_{6+x}$ causes the appearance of two characteristic plateaux at 60 K and 90 K in the T_c vs. x dependence.)

The next group [50–52] of experiments focussed on the "region of coexistence" in $YBa_2Cu_3O_{6+x}$ was done using good quality "quenched" samples.

The typical zero-field μSR spectra obtained for several $YBa_2Cu_3O_{6+x}$ samples at temperatures below 1 K are shown in Fig. 9.

The antiferromagnetic sample with $x = 0$ (the upper spectrum in Fig. 9) exhibited rather complicated spectrum with many frequencies. The dominating one was the 4 MHz frequency, the strongly damped 18 MHz and weak 2 MHz frequencies were also observed [53, 50, 47].

The sample with $x = 0.5$ shows a highly damped spin precession indicating the presence of internal magnetic fields.

For the sample with $x = 0.7$ and superconducting transition temperature of 55 K the μSR spectrum could be fitted with a single Kubo–Toyabe function. That means that the whole relaxation can be fully described by interaction of μ^+ spin

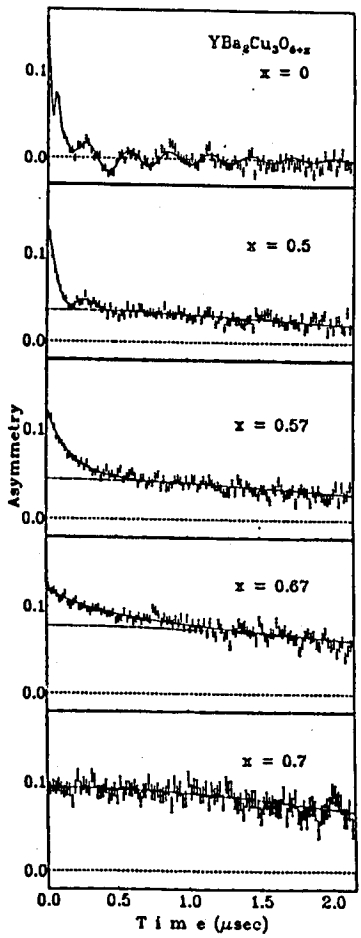

Fig. 9. μSR spectra for $YBa_2Cu_3O_{6+x}$ samples with different oxygen stoichiometry [52].

with static nuclear magnetic moments.

In the intermediate region between $x = 0.5$ and 0.7 the asymmetry is described by a sum of two parts: the the static Kubo–Toyabe and exponentially decaying. All three important parameters: 1) the fraction of exponentially relaxing component, 2) the characteristic temperature, when the magnetic correlations become visible and 3) the magnitude of internal magnetic field (as derived from the parameter λ) decrease gradually with increasing x. All of them approach zero for $x \approx 0.7$ and $T_c \approx 55$ K [52].

The phase diagram of $YBa_2Cu_3O_{6+x}$ derived from this data is shown in Fig. 10. These data confirm the statement that the magnetic correlations coexist with the superconductivity. However, the μSR method is not able to detect any

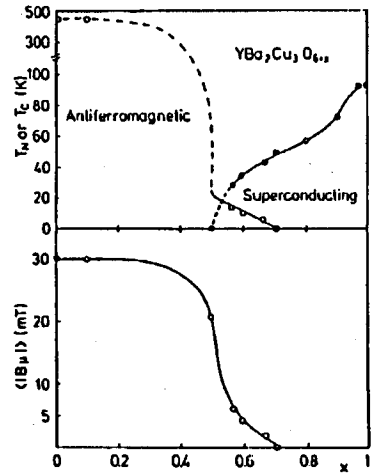

Fig. 10. Phase diagram of quenched $YBa_2Cu_3O_{6+x}$ samples [52].

trace of magnetic correlations for materials with T_c exceeding 55 K.

Another interesting group of μSR experiments was done on hydrogen loaded $YBa_2Cu_3O_{6+x}$ [54–56]. It was shown that the carrier concentration in $YBa_2Cu_3O_7$ decreases linearly with increasing hydrogen concentration. At the hydrogen concentrations greater than 0.5 hydrogen atom per unit cell, the magnetic phase appears. This phase seems to be the same as those observed in $YBa_2Cu_3O_6$.

Two frequencies of the spontaneous oscillations 4 MHz and 2 MHz were observed. The amplitude ratio for those frequencies changes monotonously with the oxygen stoichiometry of the initial material. Such dependence means that the relative occupancy of the two possible muon stopping sites changes, with the change of oxygen population in Cu–O chains.

4.3. Other groups of HTSC

The similar phase diagrams as those for $La_{2-x}Sr_xCuO_4$ and $YBa_2Cu_3O_{6+x}$ were found in bismuth based and *n*-type HTSC.

In $Bi_2Sr_2Ca_xY_{1-x}Cu_2O_8$ [57–59] or $Bi_2Sr_{2+x}Y_{1-x}Cu_2O_8$ [60] systems the carrier concentration was varied by yttrium doping. The antiferromagnetic state was observed with multiple μSR frequencies at low temperatures (0.4 MHz, 3.6 MHz, 4.4 MHz and 12 MHz). For $x = 0$, T_N was about 350 K. T_N decreases with decreasing x (increasing in carrier concentrations) and reaches 10 K at $x = 0.3$. Some kind of spin-glass-like behavior at the temperatures of about 10 K exists till $x = 0.5$, when superconductivity appears [60].

For *p*-type high T_c superconductors like $Nd_{2-x}Ce_xCuO_{4-y}$ (with $T_c \approx 25$ K for $x = 0.15$) the μSR studies [61, 62] found also the magnetic signals. The main difference of this diagram from those for $La_{2-x}Sr_xCuO_4$ is the fact that the Néel temperature remains high till $x = 0.14$ ($T_N \approx 80$ K) and drops rapidly only, when

superconductivity appears (for $x \approx 0.15$). In perfectly superconducting samples no μSR signal from electron spins (strongly damped) was observed.

5. Question of coexistence

The main experimental facts presented in Secs. 4.1 and 4.2, which could be interpreted as signature of coexistence of superconductivity and magnetic correlation in HTSC, are summarized below:

1. The exponentially damped component of the zero-field μSR depolarization function was found in superconducting samples of $La_{2-x}Sr_xCuO_4$ and $YBa_2Cu_3O_{6+x}$ at sufficiently low temperatures. The high damping rate of this component must be caused by the magnetic moments of electron origin (nuclear moments are too small). The exponential damping means that either the fields are dynamic or if they are static, their distribution is Lorentzian.
2. For $La_{2-x}Sr_xCuO_4$ with $x = 0.07$ and $T_c = 14$ K at the lowest temperatures the exponentially damped signal converted to strongly damped oscillations.
3. The correlation between amplitude of internal fields and T_c was found for both $La_{2-x}Sr_xCuO_4$ [63] and $YBa_2Cu_3O_{6+x}$ [52] as shown in Fig. 11.
4. In the samples with the highest T_c ($T_c > 32$ K for $La_{2-x}Sr_xCuO_4$ and $T_c > 50$ K for $YBa_2Cu_3O_{6+x}$ no strongly damped signal was observed. The whole μSR asymmetry observed in zero field experiments could be explained by the magnetic fields caused by the nuclear moments.
5. The fractions of muons influenced by this fields decrease with increasing x.

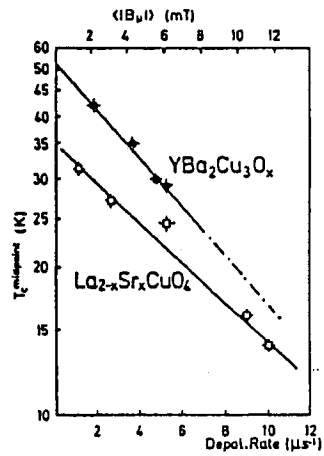

Fig. 11. Correlation between the superconducting transition temperature T_c and the internal magnetic field as measured on $La_{2-x}Sr_xCuO_4$ and $YBa_2Cu_3O_{6+x}$ [52].

The main question of the coexistence problem is, whether the superconductivity and some kind of magnetic correlations coexist in the same microscopic regions or the superconducting and magnetic phases are spatially separated.

The experiments of Brewer et al. [48] confirmed independently the "true microscopic coexistence of AFM and SC" in $YBa_2Cu_3O_{6+x}$ with x between 6.38 and 6.48. (The inhomogeneities of oxygen concentration in their samples was estimated to be smaller than $\Delta x = 0.01$.)

The absence of chemical separation does not rule out the possibility of spontaneous phase separation, where the phases differ only about the concentrations of charge carriers. The "hole rich" phase would be superconducting and "hole poor" — magnetic. Similar phase separation was also predicted for the Mott–Anderson (metal–insulator) transition in semiconductors, see e.g. [64]. For HTSC systems, Emery et al. [65] found that the diluted holes should be unstable against such phase separation.

Another strong experimental evidence of the spontaneous phase separation was found in the experiments on photo-induced superconductivity by Yu et al. [66]. The authors derived from this experiment that the photoexcited carriers condensed in hole droplets. They also observed the existence of minimum metallic conductivity as predicted by the Mott–Anderson theory.

Although we expect that such spontaneous "condensation" of charge carriers is stabilized by the fluctuations of oxygen concentration, the results of our μSR experiments would be the same, if the phase separation were not static but had dynamics slower than the muon lifetime.

6. Magnetism of Re ions

All the magnetic phenomena discussed previously considered the spin moments carried by d-electrons of Cu atoms. In this section the discussion will concern the phenomena due to the spins of the rare-earth ions present in "123" materials. The magnetic interaction between large moments of the Re^{3+} ions leads to a three dimensional magnetic ordering at very low temperatures.

The first μSR studies of such ordering were done for Gd ions [67]. In these experiments two $GdBa_2Cu_3O_{6+x}$ samples with slightly different oxygen concentrations were investigated. Their superconducting transition temperatures were 60 K and 90 K. Two frequencies of spontaneous oscillations were found in zero field μSR experiment below 2.3 K. Their temperature dependence is shown in Fig. 12. The dominant frequency in both samples was that with $\nu_{(T\to 0)} = 4.8$ MHz. A weak (with 2.5 times smaller amplitude) second frequency $\nu_{(T\to 0)} = 7.0$ MHz was observed in oxygen deficient sample ($T_c = 60$ K). In the fully oxygenated sample this frequency was hardly visible (had at least 5 times smaller amplitude). In the further experiments of Nishida et al. [68], and Dalmas de Réotier et al. [69] only the 4.8 MHz frequency was observed. It means that in fully oxygenated sample all the muons are stopped in the magnetically equivalent crystallographic sites (4.8 MHz). In oxygen deficient sample an additional muon site (7 MHz) starts to be populated.

The other $[Re]Ba_2Cu_3O_7$ systems intensively studied in μSR experiments are

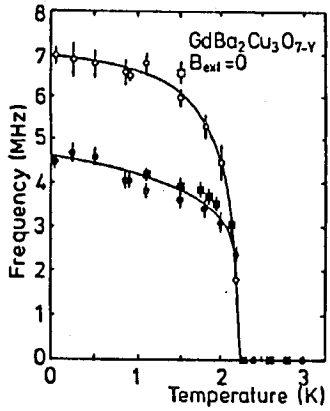

Fig. 12. Temperature dependence of the two μSR frequencies observed in $GdBa_2Cu_3O_{6+x}$. The circles are data from the 60 K sample and squares from the 90 K sample. Lines are guides for eye [67].

$HoBa_2Cu_3O_7$, see e.g. [70] and $ErBa_2Cu_3O_7$, see e.g. [71]. The magnetic ordering of the [Re] spins were found in these materials at the temperatures of 0.14 K and 0.6 K, respectively. The results of these μSR experiments point out that the magnetic phase diagram of this material is more complicated, with 2D and 3D ordering having different directions of [Re] spins.

7. Muon sites

The quantitative interpretation of μSR experiments in HTSC materials requires the identification of muon stopping sites. Like in the magnetic oxides, muons are expected to form here the muoxyl binding. So the muon site should be placed around 1 Å from the oxygen atom.

Searching for the possible muon stopping sites is based mainly on calculations of the dipolar fields. A piece of the input information for such a procedure is the magnetic structure in the ordered phase as determined e.g., from the neutron scattering experiments and the frequencies found in the μSR experiments.

Another information about the muon sites is given by the muon level-crossing experiments. In case of high-T_c superconductors such experiments were performed on ^{17}O enriched $YBa_2Cu_3O_7$ by Brewer et al. [72]. The experiment showed that the electric field gradient tensor at the oxygen closest to the muon is almost equal to that measured by NMR for the CuO_2 plane sites. However, as was discussed by Noakes [73], these results do not obviously mean that the muon is bound to the oxygen atom at the CuO_2 planes.

7.1. "214"

The Cu spins in the magnetically ordered phase of $La_{2-x}Sr_xCuO_4$ lay within the *ab* plane, as shown in Fig. 13. All present calculations of the dipolar fields in $La_{2-x}Sr_xCuO_4$ crystals [30, 31] search for the muon sites responsible for μSR oscillations with the frequency of 5.7 MHz (the internal field of 42 mT). The

muon stopping sites responsible for the non-oscillating part (the Kubo–Toyabe relaxation) were not considered. The results of these calculations show that the muons responsible for the 5.7 MIIz frequency are bound to the apical oxygen atoms as depicted in Fig. 13.

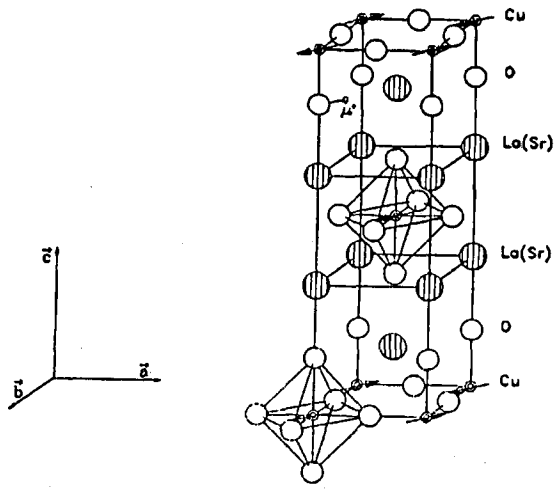

Fig. 13. The structure of antiferromagnetic phase of La_2CuO_4 and $La_{2-x}Sr_xCuO_4$ with the most probable muon stopping site.

The crystal potential calculations by Saito et al. [74] suggest however that the most stable muon site is placed further from the apical oxygen (1.57 Å), in the middle plane between the two Cu_2O planes. The authors point also to the strong supertransferred component of the magnetic field at that site.

7.2. "123"

The recently used name convention for muon stopping sites in the $YBa_2Cu_3O_{6+x}$ structure was introduced by Dawson et al. [75] with the crystal potential calculations.

As discussed in Sec. 4.2 two different sites were observed for $YBa_2Cu_3O_6$ and $YBa_2Cu_3O_7$ structures.

In the $YBa_2Cu_3O_6$ structure the muon is bound to the apical oxygen O_4 and placed about 1 Å from it. This site close to the Balmer 2 site (as proposed by Dawson et al.) is responsible for the 4.2 MIIz oscillations when Cu spins order antiferromagnetically. In case of Gd-spin ordering in oxygen deficient $GdBa_2Cu_3O_{6+x}$ the muons at this site feel the field of 52 mT (7.0 MIIz component).

In the $YBa_2Cu_3O_7$ structure the additional oxygen atoms O_1 form oxygen chains. The muons either bind directly to the chain oxygen (Lynn 12 site) or remain bound to the apical oxygen, but move towards the chain one (Balmer 1 site). Such a site is responsible for the 2.2 MIIz oscillations observed in hydrogen loaded $YBa_2Cu_3O_7$ (Cu-spin ordering), and 4.8 MIIz frequency in $GdBa_2Cu_3O_7$ (Gd-spin ordering). The positions of these sites are shown in Fig. 14.

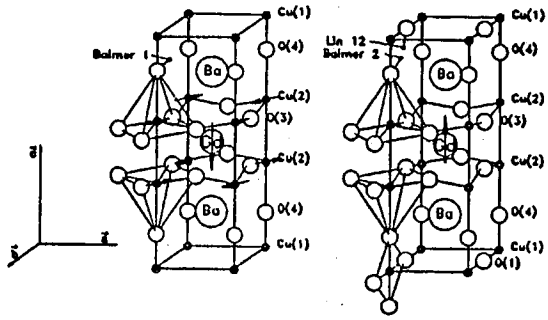

Fig. 14. The crystallographic structure of $GdBa_2Cu_3O_6$ and $GdBa_2Cu_3O_7$. The directions of Cu- and Gd-spins resulting from their antiferromagnetic ordering are showed together with the positions of the muon stopping sites.

8. Conclusions

The μSR experiments on high T_c semiconductors have shown the power of the μSR method by detection of the magnetic ordering, even in the case when magnetic moments of ions involved in such ordering are very small (here in Cu case 0.5 μ_B). μSR can very fast detect such order (by means of spontaneous oscillations in zero field). It provides also the information about ordering temperature and temperature dependence of the sublattice magnetization.

Because of its local character, μSR can detect even short range ordering with rather small coherence length.

Both above-mentioned cases (small magnetic moment, short coherence length) are difficult for neutron scattering experiments. Therefore especially in such cases μSR is competitive to the neutron scattering.

The neutron scattering experiments provide, however, more complete information on magnetic structure of the ordered state. When the quantitative interpretation of the μSR results in terms of magnetic structures requires the knowledge of the muon stopping site, what is usually not directly available.

Because of its charge muon is "much less neutral" probe in solids, comparing with neutron and often creates the phenomena specific to the muon interactions with solid, like the formation of muonium center or diffusion and trapping-detrapping processes. On the other hand the μSR studies of these processes provide information applicable also in studies of hydrogen in solids.

In conclusion we should say that μSR is a useful and powerful method in solid state physics, not competing but complementary to the neutron scattering.

Acknowledgments

This work is a result of long cooperation of the author with the group of physicists from the University of Konstanz led by Prof. Ekkehard Recknagel (Nuclear Solid State Physics Group). This cooperation and particularly the author's 21 months' stay at Konstanz was financed in parts by Bundesministerium für Forschung and Technologie and by Deutsche Forschungsgemeinschaft (SFB 306) (Germany).

All the μSR experiments were done on the accelerator facilities at the Paul –Scherrer-Institute in Villigen (Switzerland) within the projects No. RA-76-03, RA-85-17, RA-90-19.

I would like to express my gratitude to: Prof. Ekkehard Recknagel for inviting me to work in Konstanz; Prof. Alois Weidinger — the leader of μSR group at Konstanz (now at HMI Berlin) for persistent help, support and encouragement during my work in his group; my colleagues from the University of Konstanz, especially to Dr. Ch. Niedermayer and H. Glückler for close collaboration and fantastic atmosphere in our group; Prof. Joseph Budnick for supporting us with new ideas and samples prepared mainly by his co-workers from the University of Connecticut.

References

[1] A. Schenck, *Muon Spin Rotation Spectroscopy*, A. Hilger Ltd., Bristol 1985.

[2] S.F.J. Cox, *J. Phys. C* **20**, 3187 (1987).

[3] K. Nishiyama, K. Nagamine, H. Kitazawa, E. Torikai, H. Kojima, I. Tanaka, *Hyperfine Interact.* **65**, 1015 (1990); N. Nishida, S. Okuma, H. Miyatake, S. Shiratake, Y. Hidaka, T. Murakami, Y. Ueda, K. Kosuge, S. Kambe, H. Yasuoka, H. Takagi, S. Uchida, K. Nishiyama, K. Nagamine, Y. Kuno, T. Yamazaki, *ibid.* **65**, 1027 (1990); A.V. Demianov, V.S. Evseev, S. Kapusta, T.N. Mamedov, V.S. Roganov, Y.V. Obukhov, V.I. Kudinov, A.A. Evdokimov, O.P. Tkacheva, *ibid* **65**, 1035 (1990); S.G. Barsov, A.L. Gedalov, V.P. Koptev, L.A. Kuzmin, S.M. Mikirtychyants, G.V. Shcherbakov, A.A. Vasiljev, V.F. Fedotov, V.I. Kulakov, R.K. Nicolaev, N.S. Sidorov, Y.M. Mukovskii, A.S. Nigmatulin, S.E. Strunin, *ibid.* **65**, 161 (1990); H. Kitazawa, E. Torikai, K. Nishiyama, K. Nagamine, F. Iga, Y. Nishihara, *Physica C* **185-189**, 1087 (1991); N. Nishida, S. Okuma, S. Shiratake, Y. Ueda, A. Hayashi, S. Kambe, H. Yasuoka, K. Nishiyama, K. Nagamine, T. Yamazaki, *ibid.* **185-189**, 1091 (1991).

[4] B.D. Patterson, *Rev. Mod. Phys.* **60**, 69 (1988).

[5] D.K. Brice, *Phys. Lett. A* **66**, 53 (1978).

[6] R. Kubo, K. Tomita, *J. Phys. Soc. Jpn.* **9**, 888 (1954).

[7] J.G. Ivanter, V.P. Smilga, *Sov. Phys. JETP* **28**, 286 (1969).

[8] E.H. Brandt, A. Seeger, *Adv. Phys.* **35**, 189 (1986); E.H. Brandt, *Phys. Rev. Lett.* **66**, 3213 (1991).

[9] R. Kubo, T. Toyabe, in: *Magnetic Resonance and Relaxation*, Ed. R. Blinc, North Holland, Amsterdam 1967. p. 810.

[10] A. Abragam, *Compt. Rend. Acad. Sci. Ser. 2* **299**, 95 (1984).

[11] S.R. Kretzman, J.H. Brewer, D.R. Harshman, R. Keitel, D.Ll. Williams, *Phys. Rev. Lett.* **56**, 181 (1986).

[12] S.R. Kreitzman, *Hyp. Int.* **31**, 13 (1986).

[13] B.D. Patterson, A. Bosshard, U. Straumann, P. Truöl, A. Wüest, Th. Wichert, *Phys. Rev. Lett.* **52**, 938 (1984).

[14] T.L. Estle, *Hyp. Int.* **64**, 525 (1990).

[15] S.F.J. Cox, P.R. Briddon, R. Jones, *Hyp. Int.* **64**, 603 (1990).

[16] C. Boekema, *Hyp. Int.* **17–19**, 305 (1984); A. Denison, *J. Appl. Phys.* **55**, 2278 (1984).

[17] Y.M. Belousov, V.N. Gorbunov, V.P. Smilga, V.I. Fesenko, *Usp. Fiz. Nauk* **160**, 55 (1990).

[18] Y.J. Uemura, *J. Appl. Phys.* **64**, 6087 (1988); Y.J. Uemura, L.P. Le, G.M. Luke, B.J. Sternlieb, J.H. Brewer, R. Kadono, R.F. Kiefl, S.R. Kreitzman, T.M. Riseman, *Physica C* **162–164**, 857 (1989).

[19] Y.J. Uemura, L.P. Le, G.M. Luke, B.J. Sternlieb, W.D. Wu, J.H. Brewer, T.M. Rieseman, C.L. Seaman, M.B. Maple, M. Ishikawa, D.G. Hinks, J.D. Jorgensen, G. Saito, H. Yamochi, *Phys. Rev. Lett.* **66**, 2665 (1991) and references cited therein.

[20] A. Aharony, R.J. Birgenau, A. Conigilio, M.A. Kastner, H.E. Stanley, *Phys. Rev. Lett.* **60**, 1330 (1988).

[21] D.C. Johnston, J.P. Stokes, D.P. Goshorn, J.T. Lewandowski, *Phys. Rev. B* **36**, 4007 (1987).

[22] Y. Yamaguchi, A. Yamaguchi, M. Ohashi, H. Yamamoto, N. Shimoda, M. Kikuchi, Y. Syono, *Jpn. J. Appl. Phys.* **26**, L447 (1987).

[23] D. Vaknin, S.K. Sinha, D.E. Moncton, D.C. Johnston, J. Newsam, C.R. Safinya, H.E. King Jr., *Phys. Rev. Lett.* **58**, 2802 (1987).

[24] S. Mitsuda, G. Shirane, S.K. Sinha, D.C. Johnston, M.S. Alvarez, D. Vakinin, D.E. Moncton, *Phys. Rev. B* **36**, 822 (1987).

[25] Y.J. Uemura, W.J. Kossler, X.H. Yu, J.R. Kempton, H.E. Schone, D. Opie, C.E. Stronach, D.C. Johnston, M.S. Alvarez, D.P. Goshorn, *Phys. Rev. Lett.* **59**, 1045 (1987).

[26] J.I. Budnick, A. Golnik, Ch. Niedermayer, E. Recknagel, M. Rossmanith, A. Weidinger, B. Chamberland, M. Filipkowski, D.P. Yang, *Phys. Lett. A* **124**, 103 (1987).

[27] Y.J. Uemura, W.J. Kossler, J.R. Kempton, X.H. Yu, H.E. Schone, D. Opie, C.E. Stronach, J.H. Brewer, R.F. Kiefl, S.R. Kreeitzman, G.M. Luke, T. Riseman, D.Ll. Williams, E.J. Ansaldo, Y. Endoh, E. Kuno, K. Yamada, D.C. Jonston, M. Alvarez, D.P. Goshorn, Y. Hidaka, M. Oda, Y. Enomoto, M. Suzuki, T. Murakami, *Physica C* **153–155**, 769 (1988).

[28] J.I. Budnick, B. Chamberland, D.P. Yang, Ch. Niedermayer, A. Golnik, E. Recknagel, M. Rossmanith, A. Weidinger, *Europhys. Lett. A* **124**, 103 (1987).

[29] J. Saylor, L. Takacs, C. Hohenemser, J.I. Budnick, B. Chamberland, *Phys. Rev. B* **40**, 6854 (1989).

[30] L.P. Le, G.M. Luke, B.J. Sternlieb, Y.J. Uemura, J.H. Brewer, T.M. Riseman, D.C. Johnston, L.L. Miller, Y. Hidaka, H. Murakami, *Hyp. Int.* **63**, 279 (1990).

[31] B. Hitti, P. Birrer, K. Fischer, F.N. Gygax, E. Lippelt, H. Maletta, A. Schenk, M. Weber, *Hyp. Int.* **63**, 287 (1990).

[32] C.M. Soukoulis, S. Datta, Y.H. Lee, *Phys. Rev. B* 44, 446 (1991).

[33] D.R. Harshman, G. Aeppli, G.P. Espinosa, A.S. Cooper, J.P. Remeika, E.J. Ansaldo, T.M. Riseman, D.Ll. Williams, D.R. Noakes, B. Ellman, T.F. Rosenbaum, *Phys. Rev. B* **38**, 852 (1988).

[34] V.G. Grebinnik, V.N. Duginov, V.A. Zhukov, S. Kapusta, A.B. Lazarev, V.G. Olshevsky, V.Yu. Pomjakushin, S.N. Shilov, I.I. Gurevich, B.F. Kirillov, B.A. Nikolsky, A.V. Pirogov, A.N. Ponomarev, V.A. Suetin, A.G. Peresada, M.D. Nersesyan, I.P. Borovinskaya, V.R. Karasik, O.E. Omelyanovsky, T.G. Togonidze, *Physica C* **162-164**, 145 (1989); V.G. Grebinnik, V.N. Duginov, V.A. Zhukov, S. Kapusta, A.B. Lazarev, V.G. Olshevsky, V.Yu. Pomjakushin, S.N. Shilov, I.I. Gurevich, B.F. Kirillov, B.A. Nikolsky, A.V. Pirogov, A.N. Ponomarev, V.A. Suetin, I.P. Borovinskaya, M.D. Nersesyan, A.G. Peresada, Yu.F. Eltzev, V.R. Karasik, O.E. Omelyanovsky, *Hyp. Int.* **61**, 1085 (1990).

[35] J.R. Schrieffer, X.-G. Weng, S.-C. Zhang, *Phys. Rev. Lett.* **60**, 944 (1988).

[36] P. Gutsmiedl, G. Wolff, K. Andres, *Phys. Rev. B* **36**, 4043 (1987).

[37] H. Kitazawa, K. Katsumata, E. Torikai, K. Nagamine, *Solid. State Commun.* **67**, 1191 (1988); H. Kitazawa, K. Katsumata, E. Torikai, K. Nagamine, *J. Phys. (Paris) C* **8**, 2148 (1988).

[38] A. Weidinger, Ch. Niedermayer, A. Golnik, R. Simon, E. Recknagel, J.I. Budnick, B. Chamberland, C. Baines, *Phys. Rev. Lett.* **62**, 102 (1989); Ch. Niedermayer, M. Rossmanith, A. Golnik, E. Recknagel, A. Weidinger, J.I. Budnick, B. Chamberland, C. Baines, *Hyp. Int.* **51**, 593 (1989).

[39] E. Torikai, I. Tanaka, H. Kojima, H. Kitazawa, K. Nagamine, *Hyp. Int.* **63**, 271 (1990).

[40] D.R. Harshman, G. Aeppli, B. Batlogg, G.P. Espinosa, R.J. Cava, A.S. Cooper, L.W. Rupp, E.J. Ansaldo, D.Ll. Williams, *Phys. Rev. Lett.* **63**, 1187 (1989) (comment on [38]).

[41] R.F. Kiefl, J.H. Brewer, J. Carolan, P. Dosanjh, W.N. Hardy, R. Kadono, J.R. Kempton, R. Krahn, P. Schleger, B.X. Yang, Hu Zhou, G.M. Luke, B. Sternlieb, Y.J. Uemura, W.J. Kossler, X.H. Yu, E.J. Ansaldo, H. Takagi, S. Uchida, C.L. Seaman, *Phys. Rev. Lett.* **63**, 2136 (1989); R.F. Kiefl, E.J. Ansaldo, J.H. Brewer, J.F. Carolan, P. Dosanjh, W.N. Hardy, R. Kadono, J.R. Kempton, W.J. Kossler, S.R. Kreitzman, G.M. Luke, P. Schleger, C.L. Seaman, B. Sternleib, H. Takagi, S. Uchida, Y.J. Uemura, B.X. Yang, X.H. Yu, Hu Zhou, *Physica C* **162-164**, 161 (1989).

[42] K. Kumagai, T. Watanabe, K. Kawano, H. Matoba, K. Nishiyama, K. Nagamine, N. Wada, M. Okaji, K. Narra, *Physica C* 185-189, 913 (1991); G.M. Luke, L.P. Le, B.J. Sternlieb, W.D. Wu, Y.J. Uemura, J.H. Brewer, T.M. Riseman, S. Ishibashi, S. Uchida, *Physica C* **185-189**, 1175 (1991).

[43] N. Nishida, H. Miyatake, D. Shimada, S. Hikami, E. Torikai, K. Nishiyama, K. Nagamine, *Jpn. J. Appl. Phys.* **26**, L799 (1987).

[44] N. Nishida, H. Miyatake, D. Shimada, S. Okuma, M. Ishikawa, T. Takabatake, Y. Nakazawa, Y. Kuno, R. Keitel, J.H. Brewer, T.M. Riesman, D.Ll. Williams, Y. Watanabe, T. Yamazaki, K. Nishiyama, K. Nagamine, E.J. Ansaldo, E. Torikai, *Jpn. J. Appl. Phys.* **26**, L1856 (1987); N. Nishida, H. Miyatake, D. Shimada, S. Okuma, M. Ishikawa, T. Takabatake, Y. Nakazawa, Y. Kuno, R. Keitel, J.H. Brewer, T.M. Riesman, D.Ll. Williams, Y. Watanabe, T. Yamazaki, K. Nishiyama, K. Nagamine, E.J. Ansaldo, E. Torikai, *J. Phys. Soc. Jpn.* **57**, 597 (1988); N. Nishida, H. Miyatake, D. Shimada, S. Okuma, T. Yamazaki, Y. Watanabe, Y. Kuno, M. Ishikawa, T. Takabatake, K. Nagamine, K. Nishiyama, J.H. Brewer, S.R. Kreitzmann, *Physica C* 153-155, 761 (1988).

[45] J.M. Tranquada, D.E. Cox, W. Kunnmann, H. Moudden, G. Shirane, M. Suenaga, P. Zolliker, D. Vaknin, S.K. Sinha, M.S. Alvarez, A.J. Jacobson, D.C. Johnston *Phys. Rev. Lett.* **60**, 156 (1985); J. Rossat-Mignod, P. Burlet, M.J. Jurgens, J.Y. Henry, C. Vettier, *Physica C* **152**, 19 (1988).

[46] J.H. Brewer, E.J. Ansaldo, J.F. Carolan, A.C.D. Chaklader, W.N. Hardy, D.R. Harshman, M.E. Hayden, M. Ishikawa, N. Kaplan, R. Keitel, J. Kempton, R.F. Kiefl, W.J. Kossler, S.R. Kreitzman, A. Kulpa, Y. Kuno, G.M. Luke, H. Miyatake, K. Nagamine, Y. Nakazawa, N. Nishida, K. Nishiyama, S. Ohkuma, T.M. Riseman, G. Roehmer, P. Schleger, D. Shimada, C.E. Stronach, T. Takabatake, Y.J. Uemura, Y. Watanabe, D.Ll. Williaams, T. Yamazaki, B. Yang, *Phys. Rev. Lett.* **60**, 1073 (1989); G.M. Luke, R.F. Kiefl, J.H. Brewer, T.M. Riseman, D.Ll. Williams, J.R. Kempton, S.R. Kreitzman, E.J. Ansaldo, N. Kaplan, Y.J. Uemura, W.N. Hardy, J.F. Carolan, M.E. Hayden, B.X. Yang, *Physica C* **153-155**, 759 (1988).

[47] J.H. Brewer, J. Carolan, W.N. Hardy, H. Hart, R. Kadono, J. Kempton, R.F. Kiefl, S.R. Kreitzman, G.M. Luke, T.M. Riseman, P. Schleger, B.J. Sternlieb, Y.J. Uemura, D.Ll. Williams, B.X. Yang, *Physica C* **162-164**, 157 (1989).

[48] J.H. Brewer, J.F. Carolan, W.N. Hardy, B.X. Yang, P. Schleger, R. Kadono, J. Kempton, R.F. Kiefl, S.R. Kreitzman, G.M. Luke, T.M. Riseman, D.Ll. Williams, K. Chow, P. Dosanjh, B. Gowe, R. Krahn, M. Norman, *Physica C* **162-164**, 33 (1989).

[49] S. Yang, H. Claus, B.W. Veal, R. Wheeler, A.P. Paulikas, *Physica C* **193**, 243 (1992).

[50] J.I. Budnick, B. Chamberland, A. Weidinger, Ch. Niedermayer, A. Golnik, R. Simon, E. Recknagel, C. Baines, in: *Progr in High Temp. Supercond.*, Eds. L.H. Bennett, J.W. Downe, Y. Flan, G.G. Vezzali, Vol. 17, World Scientific, Singapure 1988, p.p. 206.

[51] Ch. Niedermayer, A. Golnik, H. Glückler, M. Rauer, R. Simon, E. Recknagel, A. Weidinger, J.I. Budnick, H. Eickenbusch, W. Paulus, R. Schöllhorn, *Physica C* **162-164**, 159 (1989).

[52] A. Weidinger, Ch. Niedermayer, H. Glückler, A. Golnik, G. Nowitzke, E. Recknagel, H. Eickenbusch, W. Paulus, R. Schöllhorn, J.I. Budnick, *Hyp. Int.* **63**, 147 (1990).

[53] A. Golnik, J.I. Budnick, B. Chamberland, L. Lynds, Ch. Niedermayer, F. Otter, E. Recknagel, M. Rossmanith, A. Weidinger, Z. Tan, *Physica C* **153-155**, 166 (1988).

[54] Ch. Niedermayer, H. Glückler, R. Simon, A. Golnik, M. Rauer, E. Recknagel, A. Weidinger, J.I. Budnick, W. Paulus, R. Schöllhorn, *Phys. Rev. B* **40**, 11386 (1989).

[55] H. Glückler, A. Weidinger, A. Golnik, Ch. Niedermayer, M. Rauer, R. Simon, E. Recknagel, J.I. Budnick, W. Paulus, R. Schöllhorn, *Physica C* **162-164**, 149 (1989).

[56] H. Glückler, Ch. Niedermayer, G. Nowitzke, A. Golnik, R. Simon, E. Recknagel, A. Weidinger, J. Erxmeyer, J.I. Budnick, *Hyp. Int.* **63**, 155 (1990).

[57] N. Nishida, H. Miyatake, S. Okuma, T. Tamegai, Y. Ire, R. Yoshizaki, K. Nishiyama, K. Nagamine, *Physica C* **156**, 625 (1988); N. Nishida, S. Okuma, H. Miyatake, T. Tamegai, Y. Irye, R. Yoshizaki, K. Nishiyama, K. Nagamine, R. Kadono, J.H. Brewer, *Physica C* **168**, 23 (1990).

[58] B.X. Yang, R.F. Kiefl, J.H. Brewer, J.F. Carolan, W.N. Hardy, R. Kadono, J.R. Kempton, S.R. Kreitzman, G.M. Luke, T.M. Riseman, D.Ll. Williams, Y.J. Uemura, B. Sternlieb, M.A. Subramanian, A.R. Strzelecki, J. Gopalakrishnan, A.W. Sleight, *Phys. Rev. B* **39**, 847 (1989).

[59] R. de Renzi, G. Guidi, P. Carretta, G. Calestani, S.J.F. Cox, *Phys. Lett. A* **135**, 132 (1989); R. de Renzi, G. Guidi, C. Bucci, R. Tedeschi, *Hyp. Int.* **63**, 295 (1990).

[60] B.J. Sternlieb, G.M. Luke, Y.J. Uemura, J.H. Brewer, R. Kadono, J.R. Kempton, R.F. Kiefl, S.R. Kreitzman, T.M. Riseman, D.Ll. Williams, J. Gopalakrishnan, A.W. Sleight, A.R. Strzelecki, M.A. Subramanian, *Phys. Rev. B* **40**, 11320 (1989).

[61] G.M. Luke, B.J. Sternlieb, Y.J. Uemura, J.H. Brewer, R. Kadono, R.F. Kiefl, S.R. Kreitzman, T.M. Riseman, J. Gopalakrishnan, A.W. Sleight, M.A. Subramanian, S. Uchids, H. Takagi, Y. Tokura, *Nature* **338**, 49 (1989).

[62] G.M. Luke, L.P. Le, B.J. Sternlieb, Y.J. Uemura, J.H. Brewer, R. Kadono, R.F. Kiefl, S.R. Kreitzman, T.M. Riseman, C.E. Stronach, M. Davis, S. Uchida, H. Takagi, Y. Tokura, Y. Hidaka, T. Murakami, J. Gopalakrishnan, A.W. Sleight, M.A. Subramanian, E.A. Early, J.T. Markert, M.B. Maple, C.L. Seaman, *Phys. Rev. B* **42**, 7981 (1990) and refs. cit.

[63] A. Weidinger, Ch. Niedermayer, A. Golnik, R. Simon, E.R. Recknagel, J.I. Budnick, B. Chamberland, C. Baines, *Phys. Rev. Lett.* **63**, 1188 (1989).

[64] N.F. Mott, M. Kaveh, *Adv. Phys.* **31**, 329 (1985); N.F. Mott, *Adv. Phys.* **39**, 55 (1990).

[65] V.J. Emery, S.A. Kivelson, H.Q. Lin, *Phys. Rev. Lett.* **64**, 475 (1990).

[66] G. Yu, C.H. Lee, A.J. Heeger, N. Herron, E.M. McCarron, Lin Cong, G.C. Spalding, C.A. Nordman, A.M. Goldman, *Phys. Rev. B* **45**, 4964 (1992).

[67] A. Golnik, Ch. Niedermayer, E. Recknagel, M. Rossmanith, A. Weidinger, J.I. Budnick, B. Chamberland, M. Filipkowsky, Y. Zhang, D.P. Yang, L.L. Lynds, F.A. Otter, C. Baines, *Phys. Lett. A* **125**, 71 (1987).

[68] N. Nishida, H. Miyatake, S. Okuma, Y. Kuno, Y. Watanabe, T. Yamazaki, S. Hikami, M. Ishikawa, T. Takabatake, Y. Nakazawa, S.R. Kreitzmann, J.H. Brewer, Ch.-Y. Huang, *Jpn. J. Appl. Phys.* **27**, L94 (1988).

[69] P. Dalmas de Réeotier, P. Vullet, A. Yaouanc, O. Hartmann, R. Karlsson, R. Wäppling, P. Chaudoät, S. Garçon, J.P. Sénateur, F. Weiss, T.O. Niinikoski, *Physica C* **153-155**, 1541 (1988).

[70] P. Birrer, F.N. Gygax, B. Hitti, E. Lippelt, A. Schenck, M. Weber, S. Barth, F. Hullinger, H.R. Ott, *Phys. Rev. B* **39**, 11449 (1989) and references cited therein.

[71] H. Maleta, P. Birrer, F.N. Gygax, B. Hitti, E. Lippelt, A. Schenck, M. Weber, *Hyp. Int.* **63**, 235 (1990) and references cited therein.

[72] J.H. Brewer, R.F. Kiefl, J.F. Carolan, P. Dosanjh, W.N. Hardy, S.R. Schleger, H. Zhou, E.J. Ansaldo, D.R. Noakes, L.P. Le, G.M. Luke, Y.J. Uemura, K. Hepburn-Wiley, C.E. Stronach, *Hyp. Int.* **63**, 177 (1990).

[73] D.R. Noakes, *Phys. Lett. A* **154**, 293 (1991).

[74] R. Saito, H. Kamimura, K. Nagamine, *Physica C* **185-189**, 1217 (1991).

[75] W.K. Dawson, K. Tibbs, S.P. Weathersby, C. Boekema, K.-C.B. Chan, *J. Appl. Phys.* **64**, 5809 (1988).